Journal of Materials Chemistry A

PAPER

View Article Online
View Journal

Cite this: DOI: 10.1039/c5ta05901a

Nonfullerene acceptors based on extended fused rings flanked with benzothiadiazolyl-methylenemalononitrile for polymer solar cells†

Huitao Bai,‡[ab] Yao Wu,‡[a] Yifan Wang,[bd] Yang Wu,[c] Rong Li,[a] Pei Cheng,[bd] Mingyu Zhang,[a] Jiayu Wang,[a] Wei Ma[c] and Xiaowei Zhan*[a]

Received 30th July 2015
Accepted 2nd September 2015

DOI: 10.1039/c5ta05901a

www.rsc.org/MaterialsA

Two novel A–D–A type molecules IDT–2BM and IDTT–2BM with extended fused-ring indacenodithiophene (IDT) or indacenodithienothiophene (IDTT) units as cores and strong electron-withdrawing unit 2-(benzo[*c*][1,2,5]thiadiazol-4-ylmethylene)malononitrile (BM) as the end-capping group were synthesized and investigated as electron acceptors in solution-processed polymer solar cells (PSCs). IDT–2BM and IDTT–2BM exhibited strong and broad absorption from 300 to 800 nm, and appropriate LUMO (−3.8 eV) and HOMO (−5.5 to −5.6 eV) levels matching with the classical polymer donor PBDTTT-C-T. IDT–2BM and IDTT–2BM films exhibited intrinsic electron mobilities of about 3.7×10^{-6} and 1.0×10^{-5} cm^2 V^{-1} s^{-1}, respectively. Fullerene-free PSCs employing PBDTTT-C-T as the donor and IDT–2BM or IDTT–2BM as the acceptor afforded power conversion efficiencies of 4.26% and 4.81%, respectively.

Introduction

Due to their promising application as a clean and renewable energy source, bulk-heterojunction (BHJ) organic solar cells (OSCs) have attracted much attention.[1–5] To date, an encouraging efficiency exceeding 11% has been achieved benefiting from the donor material development and device architecture improvement.[6,7] In contrast to the rapid development of donor materials, the development of electron acceptor materials has lagged behind, and most of the well-performing OSCs employed fullerene derivatives (such as $PC_{61}BM$ and $PC_{71}BM$) as electron acceptors.[4,8–10] The success of fullerene derivatives benefited from their unique properties, such as high electron affinity, high electron mobility, isotropic electron-transporting ability, and capability to form favorable nanoscale morphologies when mixed with electron donors.[11–13] However, fullerene derivatives suffer from some intrinsic drawbacks, such as weak absorption in the visible region, restricted electronic tuning and the purification problem.[14,15] OSCs composed of nonfullerene acceptors have attracted considerable attention because exploring new acceptor molecules with better optical and electronic properties will not only enrich the number of known acceptor species but also provide the possibility of obtaining better PCEs. Recently, novel nonfullerene acceptors based on rylene diimide,[16–35] diketopyrrolopyrrole,[36–40] benzothiadiazole[41–45] and other electron-withdrawing groups[46–53] have been exploited. Although the highest PCEs exceeding 6% were achieved, most of the fullerene-free OSCs yielded PCEs of <4%, which indicates that there is room for exploring novel acceptor materials.[15,54,55]

In recent years, indacenodithiophene (IDT) and indacenodithienothiophene (IDTT) units were used to construct electron donors.[56–59] The extended fused-ring unit was beneficial to π-electron delocalization, which can reduce the bandgap and broaden the absorption. In addition, the rigid coplanar structure of the molecules can prevent rotational disorder and reduce reorganization energy, which may enhance charge carrier mobility.[60,61] On the other hand, IDT and IDTT units showed special advantages in constructing electron acceptors. The LUMO levels can be readily tuned by flanking different electron-withdrawing groups. The steric effect of tetrahexylphenyl substituents on the coplanar backbone can reduce intermolecular interactions and prevent the acceptor from forming excessively large crystalline domains in BHJ films. Actually, polymer solar cells (PSCs) employing IDT and IDTT-based acceptors achieved PCEs as high as 6.31% and 6.8%, respectively.[50,51]

Among various electron-withdrawing units, 2-(benzo[*c*][1,2,5]-thiadiazol-4-ylmethylene)-malononitrile (BM) was quite attractive in synthesis of small molecule donors for vacuum-

[a]*Department of Materials Science and Engineering, College of Engineering, Key Laboratory of Polymer Chemistry and Physics of Ministry of Education, Peking University, Beijing, 100871, P. R. China. E-mail: xwzhan@pku.edu.cn*

[b]*Beijing National Laboratory for Molecular Sciences, Key Laboratory of Organic Solids, Institute of Chemistry, Chinese Academy of Sciences, Beijing, 100190, P. R. China*

[c]*State Key Laboratory for Mechanical Behavior of Materials, Xi'an Jiaotong University, Xi'an, 710049, P. R. China*

[d]*University of Chinese Academy of Sciences, Beijing, 100049, P. R. China*

† Electronic supplementary information (ESI) available: OSC device data, chemical structure of PBDTTT-C-T, TGA figures, DSC figures, XRD patterns, absorption spectra, SCLC curves, molecular orbitals and R-SoXS profiles. See DOI: 10.1039/c5ta05901a

‡ Huitao Bai and Yao Wu contributed equally.

deposited solar cells. Due to its strong electron-withdrawing ability, the BM unit can result in not only low-lying energy levels but also effective intramolecular charge transfer (ICT).[62,63] Its planar structure is beneficial to molecular stacking which will enhance charge transport. Vacuum-deposited solar cells based on BM-based molecules yielded a high efficiency exceeding 11%.[64] On the other hand, BM was used to construct electron acceptor materials due to its strong electron-withdrawing ability and low LUMO level, which can match well with classical donor materials like PBDTTT-C-T (Fig. S1, ESI†) (LUMO: −3.25 eV, HOMO: −5.11 eV).[65] However, there are only a few reports on BM-based electron acceptors for OSCs, which yielded low PCEs of <2%.[41–43]

In this work, we report design and synthesis of two novel A–D–A type acceptors (IDT–2BM and IDTT–2BM) with extended fused-ring units IDT and IDTT as cores and BM as the end-capping group, and their application in solution-processed BHJ OSCs. The PSCs based on the blends of PBDTTT-C-T:IDT–2BM and PBDTTT-C-T:IDTT–2BM afforded promising PCEs of 4.26% and 4.81%, respectively. This work reveals the great potential of the BM unit for constructing efficient nonfullerene acceptors.

Results and discussion

Materials synthesis and characterization

These two compounds were synthesized as shown in Scheme 1. IDT–2BM and IDTT–2BM were respectively synthesized through typical Stille-coupling reaction between commercially available reagents Br–BM and IDT–2SnMe$_3$ or IDTT–2SnMe$_3$ using Pd(PPh$_3$)$_4$ as the catalyst. The products were fully characterized by matrix-assisted laser desorption/ionization time-of-flight mass spectrometry (MALDI-TOF MS), ^{1}H-NMR, ^{13}C-NMR, and elemental analysis. These two compounds were readily soluble in common organic solvents, such as dichloromethane, chloroform (CF) and *o*-dichlorobenzene (*o*-DCB) at room temperature. The thermal properties of these two products were investigated by thermogravimetric analysis (TGA) and differential scanning calorimetry (DSC) methods under a nitrogen atmosphere at a heating rate of 10 °C min^{-1}. These two compounds exhibited good thermal stability with decomposition temperatures (5% weight loss) at 352 °C and 354 °C, respectively (Fig. S2 in the ESI†). According to the DSC traces (Fig. S3 in the ESI†), neither IDT–2BM nor IDTT–2BM showed melting peaks from room temperature to 320 °C. However, according to the X-ray diffraction (XRD) results (Fig. S4 in the ESI†), IDT–2BM exhibited 3 refraction peaks at 2θ = 5.50° (d spacing = 16.05 Å), 7.66° (d spacing = 11.52 Å) and 22.90° (d spacing = 3.88 Å). The peaks of 5.50° and 7.66° may be attributed to two different crystal phases, while the peak of 22.90° was attributed to π–π stacking. IDTT–2BM showed 3 peaks at 2θ = 7.72° (d spacing = 11.44 Å), 22.93° (d spacing = 3.87 Å) and 26.43° (d spacing = 3.36 Å). Among them, the peak at 7.72° was attributed to the (100) refraction, and the peak at 22.93° was attributed to the (010) refraction, while the peak at 26.43° came from the SiO$_2$/Si substrate. According to the XRD results, IDTT–2BM exhibited stronger π–π stacking than IDT–2BM, which is beneficial to electron transport.

The optical properties of these two compounds were investigated by ultraviolet-visible (UV-vis) absorption spectroscopy both in chloroform solution (Fig. S5 in the ESI†) and as thin films (Fig. 1a). The detailed data are summarized in Table 1. Benefiting from the push–pull molecule structure, two compounds exhibited broad and strong absorption from 300 nm to 800 nm in chloroform solution and as solid films. IDT–2BM and IDTT–2BM exhibited high maximum extinction coefficients of 1.2 × 10^5 M^{-1} cm^{-1} at 660 nm and 5.6 × 10^4 M^{-1}

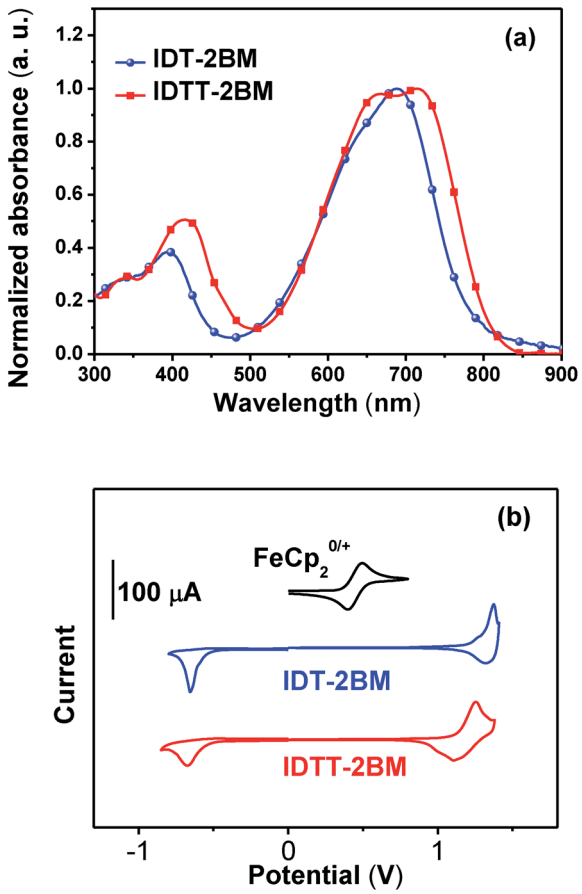

Fig. 1 (a) Absorption spectra of IDT–2BM and IDTT–2BM in films; (b) cyclic voltammograms for IDT–2BM and IDTT–2BM in CH$_3$CN/0.1 M Bu$_4$NPF$_6$ at 100 mV s^{-1}; the horizontal scale refers to an Ag/AgCl electrode as a reference electrode.

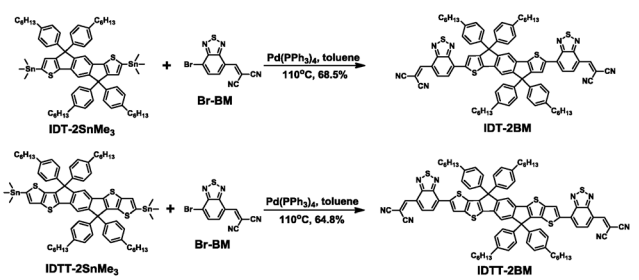

Scheme 1 The synthetic routes to IDT–2BM and IDTT–2BM.

cm^{-1} at 672 nm, respectively. Compared with IDT–2BM, IDTT–2BM showed red-shifted absorption spectra both in solution and as films, due to the increase in the conjugation length of IDTT. Relative to their solutions, the thin films of IDT–2BM and IDTT–2BM showed red-shifted absorption spectra, suggesting that some ordered structure and π–π stacking interactions existed in the films due to their coplanar backbones. The optical band gaps of IDT–2BM and IDTT–2BM estimated from the absorption edge were 1.60 eV and 1.54 eV, respectively.

The LUMO and HOMO energy levels of these two molecules were determined by the cyclic voltammetry (CV) method with the film on glassy carbon as the working electrode in acetonitrile solution containing 0.1 M Bu_4NPF_6 at a potential scan rate of 100 mV s^{-1}. As shown in Fig. 1b, both IDT–2BM and IDTT–2BM exhibited one quasi-reversible reduction wave and one irreversible oxidation wave. The onset reduction potentials of IDT–2BM and IDTT–2BM were −1.0 V *versus* $FeCp_2^{0/+}$; while the onset oxidation potentials were 0.8 V and 0.7 V *versus* $FeCp_2^{0/+}$, respectively. Assuming the absolute energy level of $FeCp_2^{0/+}$ to be 4.8 eV below vacuum,[66] LUMO levels of IDT–2BM and IDTT–2BM were calculated to be −3.8 eV and −3.8 eV, respectively; while HOMO levels were −5.6 eV and −5.5 eV, respectively. Clearly, the HOMO level of IDTT–2BM was slightly higher than that of IDT–2BM, implying that the IDTT unit had stronger electron-donating ability, while there was little difference between LUMO levels due to the same electron-withdrawing end group. The LUMO gaps (0.5 eV) and HOMO gaps (0.5 and 0.4 eV) between the donor (PBDTTT-C-T)[65] and acceptors were large enough to guarantee efficient exciton dissociation.

The intrinsic electron mobilities of IDT–2BM and IDTT–2BM were measured using the space-charge-limited current (SCLC) method with a device structure of Al/sample film/Al (Fig. S6 in the ESI†). The IDT–2BM and IDTT–2BM films exhibited average electron mobilities of 3.7×10^{-6} and 1.0×10^{-5} $cm^2\ V^{-1}\ s^{-1}$ for more than 10 devices, respectively. The higher mobility of IDTT–2BM was attributed to its more extended planar structure.

Theoretical calculation

Theoretical calculations were carried out to investigate the molecular geometries (Fig. 2) and molecular frontier orbitals (Fig. S7 in the ESI†) of IDT–2BM and IDTT–2BM and the computational details are described in the ESI.† As shown in Fig. 2, both molecules adopted a nearly flat backbone configuration, while the phenyl groups on the IDT and IDTT moieties exhibited a dihedral angle of *ca.* 115° to the backbone plane. Generally, the coplanar structure of conjugated molecules facilitated π–π stacking, which was favorable for high mobility.

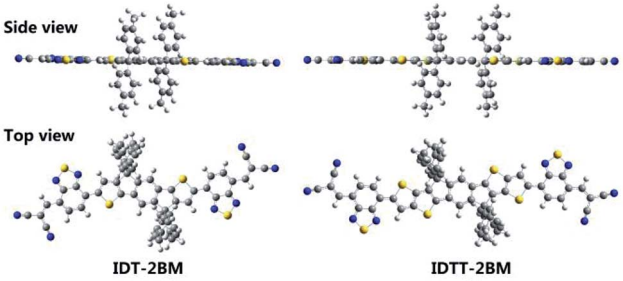

Fig. 2 Theoretical calculated optimized geometries of IDT–2BM and IDTT–2BM. The alkyl chains are replaced with methyl groups for computational simplicity.

However, the high degree of planarity and strong intermolecular interaction of parent IDT and IDTT moieties will lead to severe aggregation and large scale phase separation in blended films, finally to poor device performance. The phenyl groups on the IDT and IDTT moieties can restrict severe aggregation without reducing the backbone planarity. As shown in Fig. S7,† The HOMO and LUMO orbitals are delocalized on the whole molecular backbone.

Photovoltaic properties

To investigate the potential application of these two compounds as electron acceptors in OSCs, BHJ OSCs with a configuration of ITO/PEDOT:PSS/donor:acceptor/Ca/Al were fabricated using classical low-bandgap polymer PBDTTT-C-T as the electron donor material. Firstly, all active layers were spin-coated with a solution in *o*-DCB, and we found that the optimal D/A (PBDTTT-C-T : acceptor) ratio was 1.5 : 1 for two acceptors (Table S1 in the ESI†). To improve the morphologies and photovoltaic performance of blended films, solvent optimization was performed. 6% (v/v) of 1-chloronaphthalene (CN) was added to a *o*-DCB solution of PBDTTT-C-T:IDT–2BM, while 3% (v/v) of DIO was added to a PBDTTT-C-T:IDTT–2BM solution in a mixed solvent (*o*-DCB : CF = 3 : 2, v/v). Fig. 3a shows the *J–V* curves of the devices based on the PBDTTT-C-T : acceptor (1.5 : 1, w/w) processed under different conditions under the illumination of AM 1.5G, 100 mW cm^{-2}. Table 2 summarizes V_{OC}, short circuit current (J_{SC}), fill factor (FF), and PCE of the corresponding devices. After the addition of 6% CN, the PCE of IDT–2BM-based devices improved from 3.79% to 4.26% mainly due to the FF enhancement from 45.6% to 55.1%. After solvent optimization using *o*-DCB:CF mixed solvent and DIO additive, the V_{OC}, J_{SC} and FF of IDTT–2BM-based PSCs were improved, leading to PCE enhancement from 2.09% to 4.81%.

Table 1 Optical and electrochemical properties of IDT–2BM and IDTT–2BM

	λ_{max} [nm]					
Compound	Solution	Film	λ_{onset} [nm]	E_g^{opt} [eV]	HOMO [eV]	LUMO [eV]
IDT–2BM	660	688	775	1.60	−5.6	−3.8
IDTT–2BM	672	668, 714	805	1.54	−5.5	−3.8

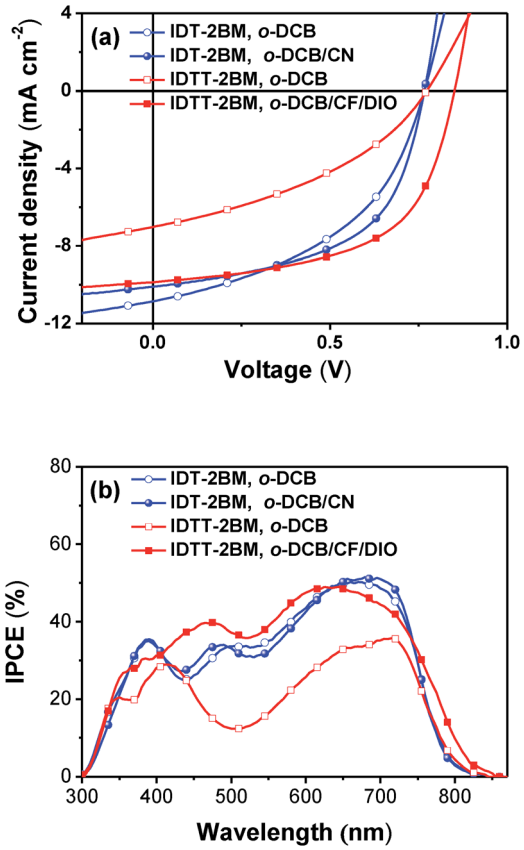

Fig. 3 (a) The J–V curves of the devices based on PBDTTT-C-T : IDT–2BM or IDTT–2BM (1.5 : 1, w/w) processed under different conditions under the illumination of AM 1.5G, 100 mW cm^{-2}; and (b) IPCE curves of corresponding devices.

As an interesting phenomenon, the V_{OC} of the device based on IDTT–2BM increased from 0.771 V to 0.845 V after solvent optimization. It may be attributed to the decreased donor concentration of the interface between the active layer and cathode, which will result in a reduced charge recombination.[67–70] Among the devices prepared under the optimal conditions, the IDTT–2BM based device showed an average V_{OC} of 0.845 V, which is 0.085 V higher than that of the IDT–2BM based device, although these two molecules possessed the same LUMO levels. In the optimal devices, the IDTT–2BM based active layer possessed a better morphology than the IDT–2BM based active layer, which resulted in less charge recombination and smaller V_{OC} loss.

The incident photons to current conversion efficiency (IPCE) curves of the corresponding devices are shown in Fig. 3b. The IPCE curves of these devices covered a broad response from 300–850 nm, and the peak values approached or exceeded 50% under optimal conditions. The J_{SC} calculated from integration of the IPCE spectra with the AM 1.5G reference spectrum was similar to that obtained from J–V measurements (the average error was 5%).

Blend film properties

To understand the influence of charge carrier transport on photovoltaic performance, electron and hole mobilities of PBDTTT-C-T : acceptor (1.5 : 1, w/w) blended films were measured by the SCLC method with the device structure: ITO/PEDOT:PSS/sample film/Au for holes and Al/sample film/Al for electrons (Fig. S8 in ESI†), and the detailed data are summarized in Table S2 in the ESI.† Before solvent optimization, PBDTTT-C-T:IDT–2BM blended films exhibited average hole and electron mobilities of 8.3×10^{-5} and 5.0×10^{-7} cm^2 V^{-1} s^{-1} (μ_h/μ_e = 166), and PBDTTT-C-T:IDTT–2BM blended films exhibited average hole and electron mobilities of 1.7×10^{-3} and 2.8×10^{-6} cm^2 V^{-1} s^{-1} (μ_h/μ_e = 607), respectively. Clearly, the hole and electron mobilities in these two blends were not balanced, which was responsible for the low FF of the devices. After the solvent optimization, the PBDTTT-C-T:IDT–2BM blended film exhibited average hole and electron mobilities of 2.5×10^{-4} and 1.0×10^{-5} cm^2 V^{-1} s^{-1} (μ_h/μ_e = 25), and the PBDTTT-C-T:IDTT–2BM blended film exhibited average hole and electron mobilities of 4.1×10^{-4} and 1.3×10^{-5} cm^2 V^{-1} s^{-1} (μ_h/μ_e = 32), respectively. Obviously, after optimization, hole and electron mobilities in the IDT–2BM system and electron mobility in the IDTT–2BM system significantly improved, and hole and electron mobilities in both blends became more balanced. The better charge transport led to enhancement of FF and thus a higher PCE.

To understand the effect of solvent optimization on the blended film morphologies, PBDTTT-C-T : acceptor (1.5 : 1, w/w) blended films were investigated using an atomic force microscope (AFM) in the tapping mode. The height and phase images of blend films fabricated with different solvents are shown in Fig. 4. Compared to the film processed without CN, PBDTTT-C-T:IDT–2BM blend films with CN additive exhibited a slightly smoother surface with the root-mean-square (RMS) roughness decreasing from 1.9 to 1.7 nm. In terms of phase

Table 2 Photovoltaic performance of the OSCs based on the PBDTTT-C-T:acceptor under the illumination of AM1.5G, 100 mW cm^{-2}

PBDTTT-C-T : acceptor (1.5 : 1, w/w)	Solution	V_{OC}[c] (V)	J_{SC}[c] (mA cm^{-2})	FF[c] (%)	PCE[c] (%)
IDT–2BM	o-DCB	0.762 ± 0.003 (0.766)	10.63 ± 0.18 (10.85)	45.2 ± 0.4 (45.6)	3.67 ± 0.12 (3.79)
	o-DCB/CN[a]	0.760 ± 0.004 (0.766)	9.81 ± 0.23 (10.10)	54.4 ± 0.5 (55.1)	4.19 ± 0.15 (4.26)
IDTT–2BM	o-DCB	0.771 ± 0.002 (0.773)	6.92 ± 0.09 (7.03)	38.1 ± 0.2 (38.5)	2.01 ± 0.06 (2.09)
	o-DCB/CF/DIO[b]	0.845 ± 0.004 (0.851)	9.67 ± 0.16 (9.87)	56.8 ± 0.4 (57.2)	4.70 ± 0.10 (4.81)

[a] o-DCB/CN = 100 : 6 (v/v). [b] o-DCB/CF/DIO = 60 : 40 : 3 (v/v). [c] The performance of the best device is given in parentheses and the average PCE was obtained from over 20 devices.

images, the blend film processed with CN exhibited a smaller size but clearer phase separation and more uniform morphology than that without CN. The clearer phase separation and more uniform morphology were beneficial to charge transport. According to the height images, the PBDTTT-C-T:IDTT–2BM blend film exhibited a smooth surface with a RMS roughness of 0.6 nm. After solvent optimization, the PBDTTT-C-T:IDTT–2BM blend film exhibited larger domains with an increased roughness of 7.8 nm.

Resonant soft X-ray scattering (R-SoXS) is further employed to probe the phase-separated morphologies of the blends in the bulk under the different conditions.[71–73] A photon energy of 283 eV was selected to provide polymer/small molecule contrast while avoiding high absorption, which would produce background fluorescence and can lead to radiation damage.[74] Fig. 5 shows the R-SoXS profiles of the PBDTTT-C-T:IDT–2BM blend films cast from *o*-DCB without or with CN and PBDTTT-C-T:IDTT–2BM blend films cast from *o*-DCB or *o*-DCB/CF/DIO. The median of the distribution s_{median} of scattering corresponds to the characteristic median length scale, ξ, of the corresponding log-normal distribution in real space with $\xi = 1/s_{median}$, a model independent statistical quantity (Fig. S10 in the ESI†). When the PBDTTT-C-T:IDT–2BM blend films are processed with pure *o*-DCB, the profile shows a low scattering intensity with a ξ of ~80 nm; when CN is used as an additive, ξ decreases to ~30–40 nm and the scattering intensity is improved. Higher integration of scattering intensity after processing with CN indicates that the phase is purer,[75] which is favorable to reduce bimolecular recombination and is thus beneficial for FF.[76] The ξ of PBDTTT-C-T:IDTT–2BM processed with pure *o*-DCB is about 40 nm. After using *o*-DCB/CF/DIO, ξ of

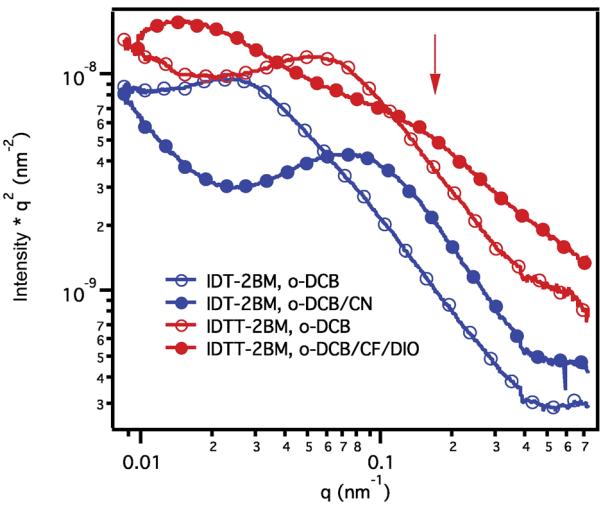

Fig. 5 R-SoXS profiles of PBDTTT-C-T:IDT–2BM processed with *o*-DCB and *o*-DCB/CN, and PBDTTT-C-T:IDTT–2BM processed with *o*-DCB and *o*-DCB/CF/DIO.

PBDTTT-C-T:IDTT–2BM decreases to ~15 nm and the integration of scattering intensity becomes higher. It is noted that the scattering of PBDTTT-C-T:IDTT–2BM processed with *o*-DCB/CF/DIO shows two peaks. The peak near $q = 0.01$ nm^{-1} originates from mass variation, which is confirmed with the scattering at 270 eV (strong material: vacuum contrast) (Fig. S9 in the ESI†). The emergence of the peak at $q = 0.2$ nm^{-1} (indicated by an arrow) at the resonant energy 283 eV indicates the phase separation between PBDTTT-C-T and IDTT–2BM. The smaller and purer domains are favorable for charge separation and transport, which will induce higher performance.[77]

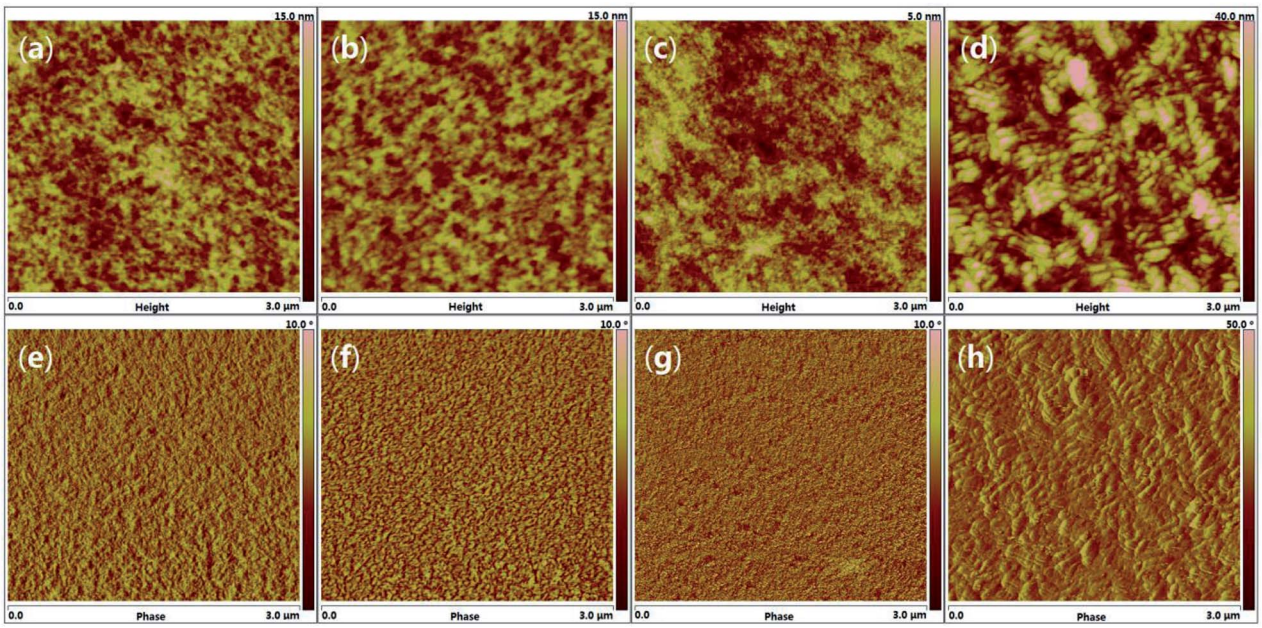

Fig. 4 AFM height (top) and phase (bottom) images (3 μm × 3 μm) of active layers: (a) and (e) PBDTTT-C-T:IDT–2BM (*o*-DCB), (b) and (f) PBDTTT-C-T:IDT–2BM (*o*-DCB, 6% CN), (c) and (g) PBDTTT-C-T:IDTT–2BM (*o*-DCB), and (d) and (h) PBDTTT-C-T:IDTT–2BM (*o*-DCB/CF, 3% DIO).

Conclusions

We developed two novel A–D–A type molecules IDT–2BM and IDTT–2BM, using extended fused-ring units IDT and IDTT as cores and electron-withdrawing unit BM as the end-capping group, and investigated their performance as electron acceptors in solution-processed PSCs. Theoretical calculations revealed that both molecules adopted a nearly flat backbone configuration with non-coplanar phenyl substituent groups, which was beneficial to forming favorable nanoscale phase separation in active layers without severe aggregation. IDT–2BM and IDTT–2BM exhibited strong and broad absorption in the visible region. IDTT–2BM exhibited red-shifted absorption relative to IDT–2BM, due to an increase in the conjugation length of IDTT. IDT–2BM and IDTT–2BM exhibited similar LUMOs (−3.8 eV) but different HOMOs (−5.6 and −5.5 eV), due to the stronger electron-donating ability of IDTT. IDTT–2BM films exhibited higher electron mobilities than IDT–2BM, due to their bigger planar structure. By optimizing the morphologies, PSCs based on PBDTTT-C-T:IDT–2BM or IDTT–2BM afforded promising PCEs of 4.26% and 4.81%, respectively. The higher PCE of IDTT–2BM-based devices was attributed to higher mobility and more suitable morphology. This work demonstrates the great potential of BM-based molecules for constructing high-efficiency fullerene-free OSCs.

Experimental section

Synthesis of IDT–2BM

To a three-necked round bottom flask were added IDT–bis-(trimethylstannane) (370 mg, 0.30 mmol), 2-((7-bromobenzo[*c*][1,2,5]thiadiazol-4-yl)methylene)malononitrile (203 mg, 0.70 mmol) and toluene (20 mL). The mixture was deoxygenated with argon for 15 min, and then $Pd(PPh_3)_4$ (40 mg, 0.034 mmol) was added. The mixture was refluxed for 24 h and then cooled to room temperature. 40 mL KF (0.1 g mL^{-1}) solution was added and stirred at room temperature overnight to remove the tin impurity. Water (150 mL) was added and the mixture was extracted with $CHCl_3$ (2 × 150 mL). The organic phase was dried over anhydrous $MgSO_4$. After removing the solvent, the residue was purified by column chromatography on silica gel using petroleum ether/$CHCl_3$ (1 : 2) as eluent yielding a blue black solid (272.5 mg, 68.5%). ^{1}H-NMR (400 MHz, CD_2Cl_2): δ 8.77 (s, 2H), 8.70 (d, J = 8 Hz, 2H), 8.29 (s, 2H), 7.98 (d, J = 8 Hz, 2H), 7.66 (s, 2H), 7.27 (d, J = 8 Hz, 8H), 7.14 (d, J = 8 Hz, 8H), 2.59 (m, 8H), 1.61 (m, 8H), 1.29 (m, 24H), 0.85 (m, 12H). ^{13}C-NMR (100 MHz, $CDCl_3$): δ 158.43, 155.05, 154.71, 152.30, 151.18, 147.85, 142.38, 141.92, 141.45, 136.30, 134.01, 130.96, 128.95, 128.19, 126.95, 123.69, 121.49, 118.84, 114.42, 113.64, 81.87, 63.58, 35.91, 32.04, 31.69, 29.46, 22.92, 14.42. MS (MALDI-TOF): m/z 1326 (M^+). Anal. calcd for $C_{84}H_{78}N_8S_4$: C, 75.98; H, 5.92; N, 8.44. Found: C, 76.07; H, 5.85; N, 8.48%. $\lambda_{max,s}$ = 660 nm (1.2 × 10^5 M^{-1} cm^{-1}).

Synthesis of IDTT–2BM

To a three-necked round bottom flask were added IDTT–bis-(trimethylstannane) (201.8 mg, 0.15 mmol), 2-((7-bromobenzo[*c*][1,2,5]thiadiazol-4-yl)methylene)malononitrile (95.7 mg, 0.33 mmol) and toluene (20 mL). The mixture was deoxygenated with argon for 15 min, and then $Pd(PPh_3)_4$ (40 mg, 0.034 mmol) was added. The mixture was refluxed for 24 h and then cooled to room temperature. 40 mL of KF (0.1 g mL^{-1}) solution was added and stirred at room temperature overnight to remove the tin impurity. Water (150 mL) was added and the mixture was extracted with $CHCl_3$ (2 × 150 mL). The organic phase was dried over anhydrous $MgSO_4$. After removing the solvent, the residue was purified by column chromatography on silica gel using petroleum ether/$CHCl_3$ (1 : 2) as eluent yielding a blue black solid (140 mg, 64.8%). ^{1}H-NMR (400 MHz, CD_2Cl_2): δ 8.78 (s, 2H), 8.73 (s, 2H), 8.68 (d, J = 8 Hz, 2H), 7.91 (d, J = 8 Hz, 2H), 7.66 (s, 2H), 7.26 (d, J = 8 Hz, 8H), 7.16 (d, J = 8 Hz, 8H), 2.59 (m, 8H), 1.56 (m, 8H), 1.26 (m, 24H), 0.84 (m, 12H). ^{13}C-NMR (100 MHz, $CDCl_3$): δ 154.51, 154.33, 151.88, 150.77, 147.30, 146.81, 143.85, 142.24, 139.60, 136.84, 136.54, 133.27, 130.58, 128.75, 127.99, 125.19, 123.55, 121.23, 117.68, 114.06, 113.20, 81.53, 63.04, 35.59, 31.67, 31.25, 29.14, 22.55, 14.05. MS (MALDI-TOF): m/z 1438.6 (M^+). Anal. calcd for $C_{88}H_{78}N_8S_6$: C, 73.40; H, 5.46; N, 7.78. Found: C, 73.14; H, 5.70; N, 7.57%. $\lambda_{max,s}$ = 672 nm (5.6 × 10^4 M^{-1} cm^{-1}).

Characterization

The ^{1}H and ^{13}C-NMR spectra were recorded using a Bruker AVANCE 400 MHz spectrometer employing tetramethylsilane (TMS; δ = 0 ppm) as an internal standard. Elemental analysis was carried out using a Flash EA 1112 elemental analyzer. Mass spectra were recorded using a Bruker Daltonics Biflex III MALDI-TOF Analyzer in the MALDI mode. Solution (chloroform) and thin film (on a quartz substrate) UV-vis absorption spectra were recorded using a Jasco V-570 spectrophotometer. Electrochemical measurements were carried out under nitrogen in a deoxygenated solution of tetra-*n*-butylammonium hexafluorophosphate (0.1 M) in acetonitrile using a potential scan rate of 100 mV s^{-1} employing a computer-controlled Zahner IM6e electrochemical workstation, a glassy-carbon working electrode coated with the acceptor film, a platinum-wire auxiliary electrode, and an Ag/AgCl electrode as a reference electrode. The potentials were referenced to a ferrocenium/ferrocene ($FeCp_2^{0/+}$) couple using ferrocene as an external standard. Thermogravimetric analysis (TGA) measurements were performed using a Shimadzu thermogravimetric analyzer (Model DTG-60) under flowing nitrogen gas at a heating rate of 10 °C min^{-1}. Differential scanning calorimetry (DSC) measurements were performed using a Mettler differential scanning calorimeter (DSC822e) under nitrogen gas at a heating rate of 10 °C min^{-1}. Wide angle X-ray diffraction of the thin films was performed in the reflection mode at 40 kV and 200 mA using Cu-Kα radiation in a 2 kW Rigaku D/max-2500 X-ray diffractometer. The nanoscale morphology of the blend films was observed using a Veeco Nanoscope V atomic force microscope (AFM) in the tapping mode.

Fabrication and characterization of photovoltaic cells

Organic solar cells were fabricated with the structure ITO/PEDOT:PSS/PBDTTT-C-T:acceptor/Ca/Al. The patterned indium tin oxide (ITO) glass (sheet resistance = 15 Ω sq^{-1}) was pre-cleaned in an ultrasonic bath of acetone and isopropanol,

and treated in an ultraviolet-ozone chamber (Jelight Company, USA) for 23 min. A thin layer (35 nm) of poly(3,4-ethylenedioxythiophene):poly(styrene sulfonate) (PEDOT:PSS, Baytron PVP AI 4083, Germany) was spin-coated onto the ITO glass and baked at 150 °C for 20 min. A PBDTTT-C-T:IDT–2BM mixture (30 mg mL^{-1} in total) in *o*-DCB without or with 6% (v/v) CN, or a PBDTTT-C-T:IDTT–2BM mixture (30 mg mL^{-1} in total) in *o*-DCB or *o*-DCB/CF/DIO (60/40/3, v/v) was spin-coated on the PEDOT:PSS layer to form a photosensitive layer. The calcium layer (*ca.* 20 nm) and the aluminum layer (*ca.* 100 nm) were then evaporated onto the surface of the photosensitive layer under vacuum (*ca.* 10^{-5} Pa) to form the negative electrode. The active area of the device was 4 mm^2. The *J–V* curve was measured using a computer-controlled B2912A Precision Source/Measure Unit (Agilent Technologies). An XES-70S1 (SAN-EI Electric Co., Ltd) solar simulator (AAA grade, 70 × 70 mm^2 photobeam size) coupled with AM 1.5 G solar spectrum filters was used as the light source, and the optical power at the sample was 100 mW cm^{-2}. A 2 × 2 cm^2 monocrystalline silicon reference cell (SRC-1000 TC-QZ) was purchased from VLSI Standards Inc. The IPCE spectrum was measured using a solar cell spectral response measurement system QE-R3011 (Enlitech Co., Ltd). The light intensity at each wavelength was calibrated using a standard single crystal Si photovoltaic cell. Hole-only or electron-only diodes were fabricated using the architectures ITO/PEDOT:PSS/active layer/Au for holes and Al/active layer/Al for electrons. The mobility was extracted by fitting the current density–voltage curves using the Mott–Gurney relationship (space charge limited current).

Computational details

Density functional theory calculations were performed with the Gaussian 09 program,[78] using the B3LYP functional.[79,80] All-electron double-ξ valence basis sets with polarization functions 6-31G* were used for all atoms.[81] Geometry optimizations were performed with full relaxation of all atoms in the gas phase without solvent effects. Vibration frequency calculation was performed to check that the stable structures had no imaginary frequency. Charge distribution of the molecules was calculated by Mulliken population analysis.

Acknowledgements

We thank the NSFC (91433114 and 51261130582) and the 973 Program (2011CB808401) for financial support. We gratefully acknowledge the Supercomputing Center of the Chinese Academy of Sciences for the theoretical calculation service. X-ray data were acquired at beamlines 11.0.1.2 (ref. 82) at the Advanced Light Source, which is supported by the Director, Office of Science, Office of Basic Energy Sciences, of the U.S. Department of Energy under Contract No. DE-AC02-05CH11231.

Notes and references

1 Y.-J. Cheng, S.-H. Yang and C.-S. Hsu, *Chem. Rev.*, 2009, **109**, 5868.
2 Y. Li, *Acc. Chem. Res.*, 2012, **45**, 723.
3 G. Li, R. Zhu and Y. Yang, *Nat. Photonics*, 2012, **6**, 153.
4 Y. Chen, X. Wan and G. Long, *Acc. Chem. Res.*, 2013, **46**, 2645.
5 Z.-G. Zhang and Y. Li, *Sci. China: Chem.*, 2015, **58**, 192.
6 C.-C. Chen, W.-H. Chang, K. Yoshimura, K. Ohya, J. You, J. Gao, Z. Hong and Y. Yang, *Adv. Mater.*, 2014, **26**, 5670.
7 H. Zhou, Y. Zhang, C.-K. Mai, S. D. Collins, G. C. Bazan, T.-Q. Nguyen and A. J. Heeger, *Adv. Mater.*, 2015, **27**, 1767.
8 L. Ye, S. Zhang, L. Huo, M. Zhang and J. Hou, *Acc. Chem. Res.*, 2014, **47**, 1595.
9 Y. Lin, Y. Li and X. Zhan, *Chem. Soc. Rev.*, 2012, **41**, 4245.
10 J. E. Anthony, A. Facchetti, M. Heeney, S. R. Marder and X. Zhan, *Adv. Mater.*, 2010, **22**, 3876.
11 Y. He and Y. Li, *Phys. Chem. Chem. Phys.*, 2011, **13**, 1970.
12 G. Yu, J. Gao, J. C. Hummelen, F. Wudl and A. J. Heeger, *Science*, 1995, **270**, 1789.
13 T. Liu and A. Troisi, *Adv. Mater.*, 2013, **25**, 1038.
14 P. Sonar, J. P. F. Lim and K. L. Chan, *Energy Environ. Sci.*, 2011, **4**, 1558.
15 Y. Lin and X. Zhan, *Mater. Horiz.*, 2014, **1**, 470.
16 X. Zhan, Z. Tan, B. Domercq, Z. An, X. Zhang, S. Barlow, Y. Li, D. Zhu, B. Kippelen and S. R. Marder, *J. Am. Chem. Soc.*, 2007, **129**, 7246.
17 X. Zhang, Z. Lu, L. Ye, C. Zhan, J. Hou, S. Zhang, B. Jiang, Y. Zhao, J. Huang, S. Zhang, Y. Liu, Q. Shi, Y. Liu and J. Yao, *Adv. Mater.*, 2013, **25**, 5791.
18 Y. Lin, Y. Wang, J. Wang, J. Hou, Y. Li, D. Zhu and X. Zhan, *Adv. Mater.*, 2014, **26**, 5137.
19 D. Mori, H. Benten, I. Okada, H. Ohkita and S. Ito, *Energy Environ. Sci.*, 2014, **7**, 2939.
20 L. Ye, W. Jiang, W. Zhao, S. Zhang, D. Qian, Z. Wang and J. Hou, *Small*, 2014, **10**, 4658.
21 Y. Zhou, T. Kurosawa, W. Ma, Y. Guo, L. Fang, K. Vandewal, Y. Diao, C. Wang, Q. Yan, J. Reinspach, J. Mei, A. L. Appleton, G. I. Koleilat, Y. Gao, S. C. Mannsfeld, A. Salleo, H. Ade, D. Zhao and Z. Bao, *Adv. Mater.*, 2014, **26**, 3767.
22 Y. Zang, C.-Z. Li, C.-C. Chueh, S. T. Williams, W. Jiang, Z.-H. Wang, J.-S. Yu and A. K.-Y. Jen, *Adv. Mater.*, 2014, **26**, 5708.
23 J. Zhao, Y. Li, H. Lin, Y. Liu, K. Jiang, C. Mu, T. Ma, J. Y. Lin Lai, H. Hu, D. Yu and H. Yan, *Energy Environ. Sci.*, 2015, **8**, 520.
24 C. Mu, P. Liu, W. Ma, K. Jiang, J. Zhao, K. Zhang, Z. Chen, Z. Wei, Y. Yi, J. Wang, S. Yang, F. Huang, A. Facchetti, H. Ade and H. Yan, *Adv. Mater.*, 2014, **26**, 7224.
25 H. Li, T. Earmme, G. Ren, A. Saeki, S. Yoshikawa, N. M. Murari, S. Subramaniyan, M. J. Crane, S. Seki and S. A. Jenekhe, *J. Am. Chem. Soc.*, 2014, **136**, 14589.
26 Y. Liu, C. Mu, K. Jiang, J. Zhao, Y. Li, L. Zhang, Z. Li, J. Y. Lai, H. Hu, T. Ma, R. Hu, D. Yu, X. Huang, B. Z. Tang and H. Yan, *Adv. Mater.*, 2015, **27**, 1015.
27 O. K. Kwon, J.-H. Park, D. W. Kim, S. K. Park and S. Y. Park, *Adv. Mater.*, 2015, **27**, 1951.
28 C. Lee, H. Kang, W. Lee, T. Kim, K. H. Kim, H. Y. Woo, C. Wang and B. J. Kim, *Adv. Mater.*, 2015, **27**, 2466.
29 Y.-J. Hwang, T. Earmme, B. A. Courtright, F. N. Eberle and S. A. Jenekhe, *J. Am. Chem. Soc.*, 2015, **137**, 4424.

30 X. Zhang, C. L. Zhan and J. N. Yao, *Chem. Mater.*, 2015, **27**, 166.
31 Y. Zhong, M. T. Trinh, R. Chen, W. Wang, P. P. Khlyabich, B. Kumar, Q. Xu, C.-Y. Nam, M. Y. Sfeir, C. Black, M. L. Steigerwald, Y.-L. Loo, S. Xiao, F. Ng, X.-Y. Zhu and C. Nuckolls, *J. Am. Chem. Soc.*, 2015, **136**, 15215.
32 X. Zhan, A. Facchetti, S. Barlow, T. J. Marks, M. A. Ratner, M. R. Wasielewski and S. R. Marder, *Adv. Mater.*, 2011, **23**, 268.
33 P. Cheng, L. Ye, X. Zhao, J. Hou, Y. Li and X. Zhan, *Energy Environ. Sci.*, 2014, **7**, 1351.
34 Y. Lin, J. Wang, S. Dai, Y. Li, D. Zhu and X. Zhan, *Adv. Energy Mater.*, 2014, **4**, 1400420.
35 Y. Cai, L. Huo, X. Sun, D. Wei, M. Tang and Y. Sun, *Adv. Energy Mater.*, 2015, **5**, 1500032.
36 Y. Lin, Y. Li and X. Zhan, *Adv. Energy Mater.*, 2013, **3**, 724.
37 H. Bai, P. Cheng, Y. Wang, L. Ma, Y. Li, D. Zhu and X. Zhan, *J. Mater. Chem. A*, 2014, **2**, 778.
38 W. Li, W. S. Roelofs, M. Turbiez, M. M. Wienk and R. A. Janssen, *Adv. Mater.*, 2014, **26**, 3304.
39 Y. Yang, G. Zhang, C. Yu, C. He, J. Wang, X. Chen, J. Yao, Z. Liu and D. Zhang, *Chem. Commun.*, 2014, **50**, 9939.
40 Y. Lin, P. Cheng, Y. Li and X. Zhan, *Chem. Commun.*, 2012, **48**, 4773.
41 K. B. Krueger, P. E. Schwenn, K. Gui, A. Pivrikas, P. Meredith and P. L. Burn, *Appl. Phys. Lett.*, 2011, **98**, 083301.
42 P. E. Schwenn, K. Gui, A. M. Nardes, K. B. Krueger, K. H. Lee, K. Mutkins, H. Rubinstein-Dunlop, P. E. Shaw, N. Kopidakis, P. L. Burn and P. Meredith, *Adv. Energy Mater.*, 2011, **1**, 73.
43 Y. Fang, A. K. Pandey, A. M. Nardes, N. Kopidakis, P. L. Burn and P. Meredith, *Adv. Energy Mater.*, 2013, **3**, 54.
44 J. T. Bloking, T. Giovenzana, A. T. Higgs, A. J. Ponec, E. T. Hoke, K. Vandewal, S. W. Ko, Z. N. Bao, A. Sellinger and M. D. McGehee, *Adv. Energy Mater.*, 2014, **4**, 1301426.
45 S. Holliday, R. S. Ashraf, C. B. Nielsen, M. Kirkus, J. A. Rohr, C. H. Tan, E. Collado-Fregoso, A. C. Knall, J. R. Durrant, J. Nelson and I. McCulloch, *J. Am. Chem. Soc.*, 2015, **137**, 898.
46 F. G. Brunetti, X. Gong, M. Tong, A. J. Heeger and F. Wudl, *Angew. Chem., Int. Ed.*, 2010, **49**, 532.
47 T. Zhou, T. Jia, B. Kang, F. Li, M. Fahlman and Y. Wang, *Adv. Energy Mater.*, 2011, **1**, 431.
48 K. N. Winzenberg, P. Kemppinen, F. H. Scholes, G. E. Collis, Y. Shu, T. Birendra Singh, A. Bilic, C. M. Forsyth and S. E. Watkins, *Chem. Commun.*, 2013, **49**, 6307.
49 C. B. Nielsen, E. Voroshazi, S. Holliday, K. Cnops, D. Cheyns and I. McCulloch, *J. Mater. Chem. A*, 2014, **2**, 12348.
50 Y. Lin, Z.-G. Zhang, H. Bai, J. Wang, Y. Yao, Y. Li, D. Zhu and X. Zhan, *Energy Environ. Sci.*, 2015, **8**, 610.
51 Y. Lin, J. Wang, Z. G. Zhang, H. Bai, Y. Li, D. Zhu and X. Zhan, *Adv. Mater.*, 2015, **27**, 1170.
52 H. Bai, Y. Wang, P. Cheng, J. Wang, Y. Wu, J. Hou and X. Zhan, *J. Mater. Chem. A*, 2015, **3**, 1910.
53 X. Zhao and X. Zhan, *Chem. Soc. Rev.*, 2011, **40**, 3728.
54 Y. Lin and X. Zhan, *Adv. Energy Mater.*, 2015, DOI: 10.1002/aenm.201501063.
55 A. F. Eftaiha, J. P. Sun, I. G. Hill and G. C. Welch, *J. Mater. Chem. A*, 2014, **2**, 1201.
56 X. Guo, M. Zhang, J. Tan, S. Zhang, L. Huo, W. Hu, Y. Li and J. Hou, *Adv. Mater.*, 2012, **24**, 6536.
57 J. J. Intemann, K. Yao, Y.-X. Li, H.-L. Yip, Y.-X. Xu, P.-W. Liang, C.-C. Chueh, F.-Z. Ding, X. Yang, X. Li, Y. Chen and A. K. Y. Jen, *Adv. Funct. Mater.*, 2014, **24**, 1465.
58 Y.-X. Xu, C.-C. Chueh, H.-L. Yip, F.-Z. Ding, Y.-X. Li, C.-Z. Li, X. Li, W.-C. Chen and A. K.-Y. Jen, *Adv. Mater.*, 2012, **24**, 6356.
59 M. Zhang, X. Guo, X. Wang, H. Wang and Y. Li, *Chem. Mater.*, 2011, **23**, 4264.
60 H. Bai, Y. Wang, P. Cheng, Y. Li, D. Zhu and X. Zhan, *ACS Appl. Mater. Interfaces*, 2014, **6**, 8426.
61 Y. Li, K. Yao, H.-L. Yip, F.-Z. Ding, Y.-X. Xu, X. Li, Y. Chen and A. K.-Y. Jen, *Adv. Funct. Mater.*, 2014, **24**, 3631.
62 L.-Y. Lin, Y.-H. Chen, Z.-Y. Huang, H.-W. Lin, S.-H. Chou, F. Lin, C.-W. Chen, Y.-H. Liu and K.-T. Wong, *J. Am. Chem. Soc.*, 2011, **133**, 15822.
63 L.-Y. Lin, C.-W. Lu, W.-C. Huang, Y.-H. Chen, H.-W. Lin and K.-T. Wong, *Org. Lett.*, 2011, **13**, 4962.
64 X. Che, X. Xiao, J. D. Zimmerman, D. Fan and S. R. Forrest, *Adv. Energy Mater.*, 2014, **4**, 1400568.
65 L. Huo, S. Zhang, X. Guo, F. Xu, Y. Li and J. Hou, *Angew. Chem., Int. Ed.*, 2011, **50**, 9697.
66 J. Pommerehne, H. Vestweber, W. Guss, R. F. Mahrt, H. Bässler, M. Porsch and J. Daub, *Adv. Mater.*, 1995, **7**, 551.
67 B. Yang, F. Guo, Y. Yuan, Z. Xiao, Y. Lu, Q. Dong and J. Huang, *Adv. Mater.*, 2013, **25**, 572.
68 B. Yang, Y. Yuan and J. Huang, *J. Phys. Chem. C*, 2014, **118**, 5196.
69 M. Zhang, H. Wang, H. Tian, Y. Geng and C. W. Tang, *Adv. Mater.*, 2011, **23**, 4960.
70 X. Guo, M. Zhang, W. Ma, L. Ye, S. Zhang, S. Liu, H. Ade, F. Huang and J. Hou, *Adv. Mater.*, 2014, **26**, 4043.
71 W. Ma, J. R. Tumbleston, L. Ye, C. Wang, J. Hou and H. Ade, *Adv. Mater.*, 2014, **26**, 4234.
72 W. Ma, L. Ye, S. Zhang, J. Hou and H. Ade, *J. Mater. Chem. C*, 2013, **1**, 5023.
73 H. Yan, B. A. Collins, E. Gann, C. Wang and H. Ade, *ACS Nano*, 2012, **6**, 677.
74 T. Coffey, S. G. Urquhart and H. Ade, *J. Electron Spectrosc. Relat. Phenom.*, 2002, **122**, 65.
75 B. A. Collins, Z. Li, J. R. Tumbleston, E. Gann, C. R. McNeill and H. Ade, *Adv. Energy Mater.*, 2013, **3**, 65.
76 W. Ma, J. Tumbleston, M. Wang, E. Gann, F. Huang and H. Ade, *Adv. Energy Mater.*, 2013, **3**, 864.
77 L. Ye, S. Zhang, W. Ma, B. Fan, X. Guo, Y. Huang, H. Ade and J. Hou, *Adv. Mater.*, 2012, **24**, 6335.
78 M. J. Frisch, G. W. Trucks, H. B. Schlegel, G. E. Scuseria, M. A. Robb, J. R. Cheeseman, G. Scalmani, V. Barone, B. Mennucci, G. A. Petersson, H. Nakatsuji, M. Caricato, X. Li, H. P. Hratchian, A. F. Izmaylov, J. Bloino, G. Zheng, J. L. Sonnenberg, M. Hada, M. Ehara, K. Toyota, R. Fukuda, J. Hasegawa, M. Ishida, T. Nakajima, Y. Honda, O. Kitao, H. Nakai, T. Vreven, J. A. Montgomery Jr, J. E. Peralta, F. Ogliaro, M. Bearpark, J. J. Heyd, E. Brothers, K. N. Kudin, V. N. Staroverov, R. Kobayashi,

J. Normand, K. Raghavachari, A. Rendell, J. C. Burant, S. S. Iyengar, J. Tomasi, M. Cossi, N. Rega, J. M. Millam, M. Klene, J. E. Knox, J. B. Cross, V. Bakken, C. Adamo, J. Jaramillo, R. Gomperts, R. E. Stratmann, O. Yazyev, A. J. Austin, R. Cammi, C. Pomelli, J. W. Ochterski, R. L. Martin, K. Morokuma, V. G. Zakrzewski, G. A. Voth, P. Salvador, J. J. Dannenberg, S. Dapprich, A. D. Daniels, O. Farkas, J. B. Foresman, J. V. Ortiz, J. Cioslowski and D. J. Fox, *Gaussian 09, Revision A.01*, Gaussian, Inc., Wallingford CT, 2009.

79 C. T. Lee, W. T. Yang and R. G. Parr, *Phys. Rev. B: Condens. Matter Mater. Phys.*, 1988, **37**, 785.

80 A. D. Becke, *J. Chem. Phys.*, 1993, **98**, 5648.

81 R. Krishnan, J. S. Binkley, R. Seeger and J. A. Pople, *J. Chem. Phys.*, 1980, **72**, 650.

82 E. Gann, A. T. Young, B. A. Collins, H. Yan, J. Nasiatka, H. A. Padmore, H. Ade, A. Hexemer and C. Wang, *Rev. Sci. Instrum.*, 2012, **83**, 045110.